

Reconstructing bifurcation behavior of a nonlinear dynamical system by introducing weak noise

Debraj Das · Sayan Roy · Shamik Gupta

the date of receipt and acceptance should be inserted later

Abstract For a model nonlinear dynamical system, we show how one may obtain its bifurcation behavior by introducing noise into the dynamics and then studying the resulting Langevin dynamics in the weak-noise limit. A suitable quantity to capture the bifurcation behavior in the noisy dynamics is the conditional probability to observe a microscopic configuration at one time, conditioned on the observation of a given configuration at an earlier time. For our model system, this conditional probability is studied by using two complementary approaches, the Fokker-Planck and the path-integral approach. The latter has the advantage of yielding exact closed-form expressions for the conditional probability. All our predictions are in excellent agreement with direct numerical integration of the dynamical equations of motion.

1 Introduction

Nonlinear dynamical systems present a plethora of physical phenomena that are truly fascinating, but which at the same time appear counterintuitive and intriguing, especially when viewed from the perspective of linear systems that are much simpler to understand and analyze [1, 2]. As examples, one may cite chaos [3], pattern formation [4], solitons [5], and many more. Despite the intricacies and roadblocks involved in providing an analytical characterization, nonlinear phenomena have attracted the attention of physicists, engineers, biologists and mathematicians, a reason being that nature is inherently nonlinear.

Debraj Das (Equal Contribution)
Department of Physics, Ramakrishna Mission Vivekananda University, Belur Math, Howrah 711202, India

Sayan Roy (Equal Contribution)
Department of Physics, Indian Institute of Science Education and Research Bhopal, Bhopal Bypass Road, Bhauri, Bhopal 462 066, Madhya Pradesh, India

Shamik Gupta
Department of Physics, Ramakrishna Mission Vivekananda University, Belur Math, Howrah 711202, India. E-mail: shamik.gupta@rkmvu.ac.in

A very interesting dynamical feature exhibited by nonlinear systems is that of bifurcation, whereby a given dynamics exhibits qualitatively different flow structure as one or more dynamical parameters are varied. A consequence is that fixed points into which the dynamical variables settle at long times may have different stability properties for different parameter ranges, or they may even be created or destroyed as the dynamical parameters are tuned across critical values.

A deterministic dynamical system is typically characterized in terms of behavior of specific initial conditions under the dynamical evolution. In contrast, introducing noise into the dynamics requires a statistical description in the form of a suitable distribution of the dynamical variables and a study of its evolution in time. In this work, we address the issue of how one may obtain the bifurcation diagram of a nonlinear dynamical system by introducing noise into its dynamics and studying the resulting noisy dynamics using tools of stochastic processes. We show that a suitable quantity to capture the bifurcation behavior in the noisy dynamics is the conditional probability to observe a microscopic configuration of the dynamical variables at one time, conditioned on the observation of a given configuration at an earlier time. We study this conditional probability by two complementary approaches, the Fokker-Planck and the path-integral approach, with the latter offering the advantage of yielding an exact closed-form expression for the conditional probability. Our results demonstrate that when considered in the limit of weak noise, the noisy dynamics is able to reproduce the bifurcation diagram of the noiseless dynamics. Such a conclusion may not seem very surprising in retrospect, especially since in the weak-noise limit, the noisy dynamical trajectories represent small fluctuations about those for the noiseless one. Our work primarily serves as a proposal of a theoretical framework to systematically obtain the stability properties of the noiseless dynamics from a suitable analysis of the noisy one, and as an illustration of how one may derive analytical expressions of the quantities involved in the latter analysis.

The paper is laid out as follows. In Section 2, we present our model system described in terms of noiseless time evolution of a single phase-like variable on a potential landscape. We discuss some of the dynamical features of the system, and also introduce its noisy variant involving time evolution in presence of Gaussian, white noise. An analysis of the bifurcation behavior of the noiseless dynamics is taken up in Section 3. The noisy dynamics is studied in Section 4 using two independent approaches, the Fokker-Planck and the path-integral approach. In Section 5, the results obtained in the noisy dynamics in the limit of weak-noise are compared with those for the noiseless dynamics, allowing us to demonstrate how our objective of obtaining the bifurcation diagram of the noiseless dynamics from the noisy one is achieved. The paper ends with conclusions in Section 6.

2 The model

We consider a dynamical system described by a single phase-like variable $\theta \in [-\pi, \pi]$, whose time evolution is given by

$$\frac{d\theta}{dt} = A \sin \theta - B \sin 2\theta. \quad (1)$$

Here, the dynamical parameters A and B are real constants. One may get rid of one of the parameters from the dynamics by a simple rescaling of time, so that

from now on we will consider the dynamics

$$\frac{d\theta}{dt} = a \sin \theta - \sin 2\theta, \quad (2)$$

where a is a real constant.

The noisy dynamics corresponding to the noiseless evolution (2) is obtained by introducing a Gaussian, white noise term $\eta(t)$ on the right hand side of Eq. (2). One has consequently the following Langevin dynamics:

$$\frac{d\theta}{dt} = a \sin \theta - \sin 2\theta + \eta(t), \quad (3)$$

where the noise $\eta(t)$ satisfies

$$\langle \eta(t) \rangle = 0, \quad \langle \eta(t)\eta(t') \rangle = 2D\delta(t-t'), \quad (4)$$

with D a positive constant, and angular brackets denoting average over noise realizations. Note that the parameter D sets the strength of the noise, and setting it to zero reduces the noisy dynamics to the noiseless one, Eq. (2).

Equation (3) corresponds to overdamped dynamics of θ in a potential $V(\theta)$, as

$$\frac{d\theta}{dt} = -V'(\theta) + \eta(t), \quad (5)$$

with

$$V(\theta) \equiv a \cos \theta - \frac{1}{2} \cos 2\theta, \quad (6)$$

and the prime denoting first derivative with respect to θ .

Note that the potential satisfies $V_{a<0}(\theta) = V_{a>0}(\theta - \pi)$. Solving $V'(\theta) = 0$ gives for all a the solutions $\theta = 0, \pm\pi$ as well as $\theta = \cos^{-1}(a/2)$, $\sin \theta = \pm\sqrt{1 - a^2/4}$ for $-2 < a < 2$. It is easily checked that $\theta = 0$ is a maximum of $V(\theta)$ for $a > 2$ and is a minimum for $a < 2$, while $\theta = \pm\pi$ maximize $V(\theta)$ for $a < -2$ and minimize it for $a > -2$. Finally, $\theta = \cos^{-1}(a/2)$ is a maximum for $-2 < a < 2$. On the other hand, we have $V''(0) = 0$ for $a = 2$ and $V''(\pm\pi) = 0$ for $a = -2$, while $V''(\theta = \cos^{-1}(a/2); -2 < a < 2) = 0$ for $a = \pm 2$. Figure 1 shows the potential $V(\theta)$ for representative values of a .

3 Analysis of the noiseless dynamics

The fixed points θ^* of the noiseless dynamics (2) satisfy $V'(\theta^*) = 0$, and hence are given by $\theta^* = 0, \pm\pi$ for all values of a , with additional fixed points $\theta^* = \cos^{-1}(a/2)$, $\sin \theta^* = \pm\sqrt{1 - a^2/4}$ for a lying in the range $-2 < a < 2$. The linear stability of these fixed points may be determined by substituting in Eq. (2) the expansion $\theta = \theta^* + \Delta\theta$, with $|\Delta\theta|$ small, and keeping terms to linear order in $\Delta\theta$. One obtains

$$\frac{d\Delta\theta}{dt} = -V''(\theta^*)\Delta\theta. \quad (7)$$

It then follows that $V''(\theta^*) > 0$ (respectively, $V''(\theta^*) < 0$) makes the perturbation $\Delta\theta$ decay (respectively, grow) exponentially in time, rendering θ^* linearly stable (respectively, unstable). Using the properties of $V(\theta)$ discussed earlier, we conclude that

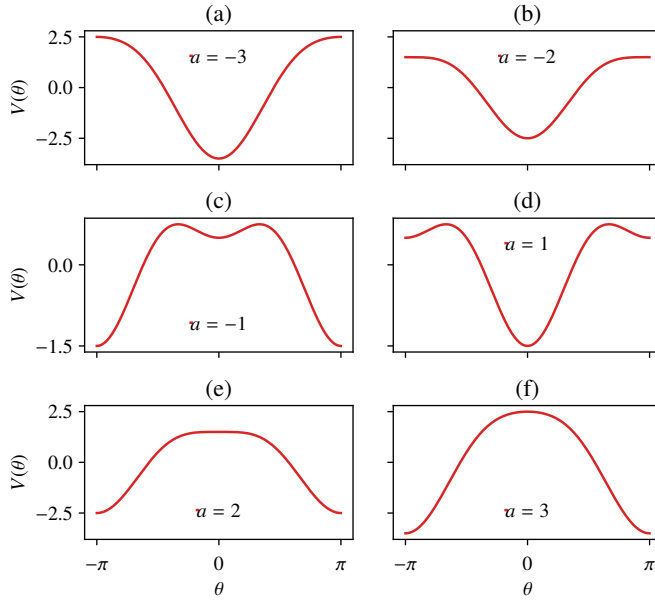


Fig. 1 (Color online) Potential $V(\theta) = a \cos \theta - (1/2) \cos 2\theta$ for representative values of the parameter a .

- For $a > 2$, the linearly stable fixed points are $\theta^* = \pm\pi$, while $\theta^* = 0$ is linearly unstable. For $a < -2$, the stability of these fixed points gets exchanged.
- For $a = 2$, the fixed point $\theta^* = 0$ is linearly neutrally stable, while $\theta^* = \pm\pi$ are linearly stable. For $a = -2$, the fixed points $\theta^* = \pm\pi$ are linearly neutrally stable, while $\theta^* = 0$ is linearly stable.
- For $-2 < a < 2$, the fixed points $\theta^* = 0, \pm\pi$ are linearly stable, while $\theta^* = \cos^{-1}(a/2)$; $\sin \theta^* = \pm\sqrt{1 - a^2/4}$ are linearly unstable.

On the basis of the foregoing, one obtains the bifurcation diagram of Fig. 2 that shows the stable (continuous blue lines) and unstable (dashed red lines) fixed points as a function of a . Coexistence of multiple stable fixed points for $-2 < a < 2$ implies hysteretic behavior for the model (2). Let us identify a 2π -periodic variable of θ as a suitable order parameter that captures this behavior. Since the stable fixed points are either zero or $\pm\pi$, one may choose $\cos \theta$ as the simplest such order parameter.

We now obtain the behavior of the stable value of $\cos \theta$ as a is tuned adiabatically from small to large values and back. Adiabatic tuning of a ensures that the system while starting from an initial state has enough time to relax to the stable state before the value of a changes appreciably. Referring to Fig. 1, if one starts with a value of a smaller than -2 , any initial θ will relax at long times to the stable fixed point at $\theta^* = 0$. As a is now adiabatically tuned to higher values, the value of θ will remain pinned to zero, until the minimum at $\theta = 0$ of the potential $V(\theta)$ turns into a maximum. The value of a at which this happens, obtained by solving $V''(0) = 0$, is given by $a = 2$. Beyond $a = 2$, the stable value of θ will change to the value at the new minima, given by $\theta = \pm\pi$. Concomitant with the

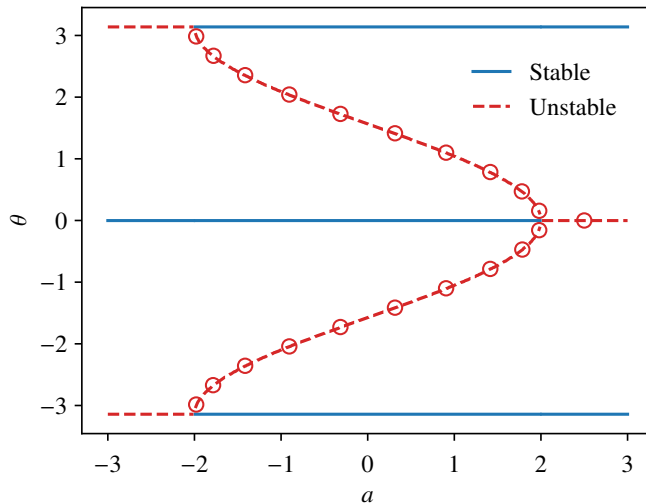


Fig. 2 (Color online) Bifurcation diagram of the noiseless dynamics (2). For all values of a , the fixed points are $\theta = 0, \pm\pi$, while for a in the range $-2 < a < 2$, additional fixed points are given by $\cos \theta = (a/2)$; stable fixed points are denoted by continuous lines, while the unstable ones are denoted by dashed lines. Here, the red circles may be obtained from the exact analysis of the noisy dynamics (3) based on the Fokker-Planck and the path-integral approach discussed in the text.

mentioned behavior, $\cos \theta$ versus a will behave as shown in Fig. 3 for the case of increasing a . Following the above line of argument, one may easily obtain the behavior of $\cos \theta$ versus a for the case when a has a starting value greater than 2 and is adiabatically decreased to a value less than -2 . The corresponding behavior is depicted in Fig. 3 for the case of decreasing a . Hysteretic behavior of $\cos \theta$ is clearly evident from the figure.

With respect to the bifurcation diagram (2), one may wonder about the nature of bifurcation at the point $(a = 2, \theta = 0)$: on decreasing a across $a = 2$, a line of unstable fixed points bifurcates into two lines of unstable fixed points that are symmetrically disposed about a line of stable fixed points. Close to the bifurcation point, expanding Eq. (2) to the first two leading orders in θ , one gets

$$\frac{d\theta}{dt} = (a - 2)\theta + (8 - a)\frac{\theta^3}{6}, \quad (8)$$

which has the form of the so-called subcritical pitchfork bifurcation [1]. Proceeding similarly, it is easy to see that the bifurcation that occurs as a is increased through $(a = -2, \theta = \pm\pi)$ is also a subcritical pitchfork bifurcation.

Figure 4 shows the dynamical trajectories for the noiseless and the noisy dynamics, Eqs. (2) and (3), respectively, from which one may observe that in the weak-noise limit ($D \rightarrow 0$), the trajectories for the noisy dynamics occur as small fluctuations ($O(\sqrt{D})$) about those for the noiseless dynamics. This observation makes us anticipate that it should be possible to extract the bifurcation behavior of the noiseless dynamics (2) from a suitable analysis of the noisy dynamics (3). A straightforward numerical check of this expectation is offered by performing numerical integration of the noisy dynamics (3) for small noise strength, obtaining

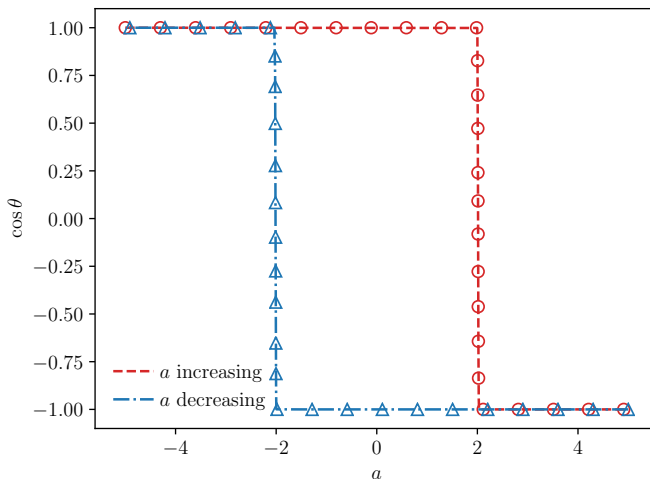


Fig. 3 (Color online) $\cos \theta$ as a function of adiabatically-tuned a , showing hysteretic behavior. The curves follow from the linear stability analysis of the noiseless dynamics (2) discussed in the text. On the other hand, the red circles and the blue triangles are obtained by numerically integrating the noisy dynamics (3) for the initial condition $\theta_0 = 0.75\pi$, and with $D = 10^{-5}$ and time step $dt = 10^{-3}$; we first let the system reach the stationary state (reached at time $t = 10$) at a given value of $a < -2$, and then increase a adiabatically to high values and back in a cycle; Here, the data correspond to one realization of the noisy dynamics.

the values of $\langle \cos \theta \rangle$ as a function of adiabatically-tuned a , and comparing with the results of the noiseless dynamics. Figure 3 indeed shows a match between the two results. Our aim in this work is to explain this match on the basis of a theoretical analysis of the noisy dynamics. We therefore turn to such an analysis in the next section.

4 Analysis of the noisy dynamics

If one has to locate dynamically the stable fixed points of the noiseless dynamics (2) for a given value of a , one needs to initiate the dynamics by specifying an initial condition for θ and then let the dynamics run for a long time in order that it relaxes to a stationary state. The latter would correspond to the stable fixed points of the dynamics. In the case of noisy dynamics (3), the system while evolving from the same initial condition will have at long times a range of possible values of θ corresponding to different dynamical trajectories attained with different realizations of the noise $\eta(t)$. In this case, it is then pertinent for an analytic characterization of the dynamics that one defines a conditional probability density $P(\theta, t|\theta_0, 0)$, which gives the probability density that the phase has the value θ at time t , given that it had the value θ_0 at the initial instant $t = 0$. Our expectation is that studying $P(\theta, t|\theta_0, 0)$ as $t \rightarrow \infty$ and $D \rightarrow 0$ should allow to recover the stable fixed points of the noiseless dynamics.

The function $P(\theta, t|\theta_0, 0)$ is 2π -periodic in both θ and θ_0 :

$$P(\theta + 2\pi, t|\theta_0 + 2\pi, 0) = P(\theta, t|\theta_0, 0), \quad (9)$$

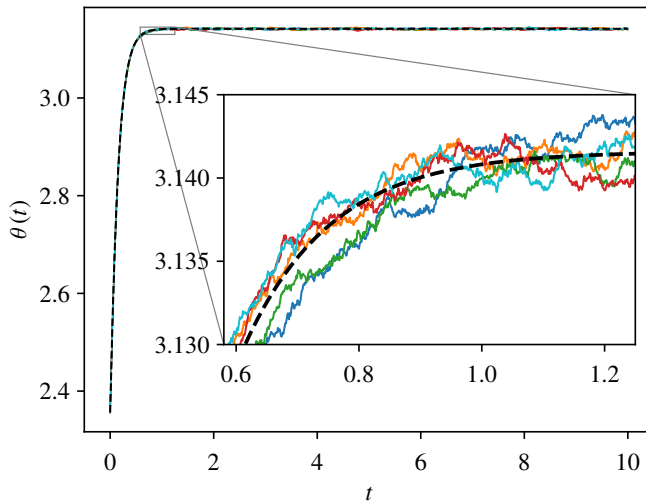


Fig. 4 (Color online) Dynamical trajectories of the noiseless and the noisy dynamics, Eqs. (2) and (3), respectively, for the initial value $\theta_0 = 0.75\pi$. The dashed line corresponds to the noiseless case, while the five continuous lines correspond to five independent realizations of the noisy dynamics. The trajectories are obtained by numerically integrating the corresponding equation of motion with integration time step $dt = 10^{-3}$ [6]. Here, we have chosen $a = 5$, $D = 10^{-5}$. One may observe that the trajectories for the noisy case represent small fluctuations ($\sim \sqrt{D}$) about the noiseless trajectory.

and obeys the normalization

$$\int_{-\pi}^{\pi} d\theta P(\theta, t|\theta_0, 0) = 1 \quad \forall \theta_0, t. \quad (10)$$

4.1 The Fokker-Planck approach

In this subsection, we discuss how one may obtain for a given value of θ_0 the conditional probability density $P(\theta, t|\theta_0, 0)$ as a function of t by solving the time evolution equation it satisfies. The time evolution of P is given by a Fokker-Planck equation that may be written down straightforwardly by using the Langevin equation (5). One gets

$$\frac{\partial P(\theta, t|\theta_0, 0)}{\partial t} = -\frac{\partial}{\partial \theta} [-V'(\theta)P(\theta, t|\theta_0, 0)] + D\frac{\partial^2 P(\theta, t|\theta_0, 0)}{\partial \theta^2}, \quad (11)$$

with the initial condition

$$P(\theta, 0|\theta_0, 0) = \delta(\theta - \theta_0). \quad (12)$$

In order to solve Eq. (11), noting that P is 2π periodic in θ , one may expand it in a Fourier series in θ :

$$P(\theta, t|\theta_0, 0) = \sum_{n=-\infty}^{\infty} \tilde{P}_n(t|\theta_0, 0)e^{in\theta}, \quad (13)$$

with $P(\theta, t|\theta_0, 0)$ being real implying that $[\tilde{P}_n(t|\theta_0, 0)]^* = \tilde{P}_{-n}(t|\theta_0, 0)$, and star denoting complex conjugation. Substituting in Eq. (11), one obtains the time evolution of the Fourier coefficients \tilde{P}_n as

$$\begin{aligned} \frac{\partial \tilde{P}_n(t|\theta_0, 0)}{\partial t} &= -Dn^2 \tilde{P}_n(t|\theta_0, 0) \\ &+ \frac{na}{2} \left[\tilde{P}_{n+1}(t|\theta_0, 0) - \tilde{P}_{n-1}(t|\theta_0, 0) \right] + \frac{n}{2} \left[\tilde{P}_{n-2}(t|\theta_0, 0) - \tilde{P}_{n+2}(t|\theta_0, 0) \right], \end{aligned} \quad (14)$$

with Eq. (12) yielding

$$\tilde{P}_n(0|\theta_0, 0) = \frac{1}{2\pi} e^{-in\theta_0}. \quad (15)$$

For any n , the system of coupled equations (14) is not closed and in fact involves an infinite hierarchy: for a given value of θ_0 , to obtain $\tilde{P}_n(t|\theta_0, 0)$ as a function of t requires knowing \tilde{P}_{n+1} and \tilde{P}_{n+2} whose solution requires knowing \tilde{P}_{n+3} and \tilde{P}_{n+4} , and so on. For the initial condition (15), however, the system of equations may be solved easily by truncating it at a given value $n = n_{\max}$, i.e., by stipulating that $\tilde{P}_n(t|\theta_0, 0) = 0$ for $n > n_{\max}$ and for all t . Here, n_{\max} may be chosen to be as large as possible.

4.2 The path-integral approach

We now discuss a complementary approach to obtain $P(\theta, t|\theta_0, 0)$ as a function of t , by invoking the Feynman-Kac path-integral formalism of treating stochastic processes [7,8,9,10]. An advantage is that in contrast to the Fokker-Planck approach, one obtains in this approach a closed-form expression for $P(\theta, t|\theta_0, 0)$. To this end, we **follow the general procedure discussed in Ref. [12]** and consider a representation of the dynamics (5) in discrete times $t_i = i\Delta t$, with $i = 0, 1, 2, \dots$, and $\Delta t > 0$ being a small time step. The discrete-time dynamics is given by

$$\theta_i = \theta_{i-1} + \Delta t \left(\bar{F}(\theta_i) + \eta_i \right), \quad (16)$$

where we have defined

$$F(\theta_i) \equiv -V'(\theta_i), \quad (17)$$

which for our model system (3) equals $F(\theta_i) = a \sin \theta_i - \sin 2\theta_i$ and $\bar{F}(\theta_i) \equiv (F(\theta_{i-1}) + F(\theta_i))/2$. In writing Eq. (16), we have used the Stratonovich rule [11] in discretizing the dynamics (3). The time-discretized Gaussian, white noise η_i satisfies $\langle \eta_i \eta_j \rangle = \sigma^2 \delta_{ij}$, where σ^2 is a positive constant with the dimension of [time – squared]⁻¹. In particular, the joint probability distribution of occurrence of a given realization $\{\eta_i\}_{1 \leq i \leq N}$ of the noise, with N being a positive integer, is given by

$$P[\{\eta_i\}] = \left(\frac{1}{2\pi\sigma^2} \right)^{N/2} \exp \left(-\frac{1}{2\sigma^2} \sum_{i=1}^N \eta_i^2 \right). \quad (18)$$

From the discrete-time dynamics (16) and the joint distribution (18), the probability of occurrence of a given phase trajectory $\{\theta_i\}_{0 \leq i \leq N} \equiv \{\theta_0, \theta_1, \theta_2, \dots, \theta_{N-1}, \theta_N = \theta\}$ is obtained as

$$P[\{\theta_i\}] = \det(\mathcal{J}) \left(\frac{1}{2\pi\sigma^2} \right)^{N/2} \prod_{i=1}^N \exp \left(-\frac{(\theta_i - \theta_{i-1} - \bar{F}(\theta_i)\Delta t)^2}{2\sigma^2(\Delta t)^2} \right). \quad (19)$$

Here, \mathcal{J} is the Jacobian matrix for the transformation $\{\eta_i\} \rightarrow \{\theta_i\}$, and is given by $\mathcal{J}_{1 \leq i, j \leq N} \equiv (\partial \eta_i / \partial \theta_j)$. For small Δt , using $\det(\mathcal{J}) = (1/\Delta t)^N \exp\left(-\sum_{i=1}^N (\Delta t/2) F'(\theta_i)\right)$, one gets by considering all possible trajectories that the probability density that the phase while starting at the value θ_0 at time $t = 0$ evolves to the value θ at time $t = N\Delta t$ is given by [12]

$$P(\theta, t|\theta_0, 0) = \left(\frac{1}{2\pi\sigma^2(\Delta t)^2}\right)^{N/2} \prod_{i=1}^{N-1} \int_{-\pi}^{\pi} d\theta_i \times \exp\left(-\Delta t \sum_{i=1}^N \left[\frac{[(\theta_i - \theta_{i-1} - \bar{F}(\theta_i)\Delta t)/\Delta t]^2}{2\sigma^2\Delta t} + \frac{F'(\theta_i)}{2}\right]\right). \quad (20)$$

In the limit of continuous time (i.e., $\Delta t \rightarrow 0$), using $D \equiv \lim_{\sigma^2 \rightarrow \infty, \Delta t \rightarrow 0} (\sigma^2/2)\Delta t$, and defining $\mathcal{D}\theta(t) \equiv \lim_{N \rightarrow \infty} \left(1/(4\pi D\Delta t)\right)^{N/2} \prod_{i=1}^{N-1} \int_{-\pi}^{\pi} d\theta_i$, one gets an exact expression for the corresponding probability density to be given by the following path integral [12]:

$$P(\theta, t|\theta_0, 0) = \int_{\theta(0)=\theta_0}^{\theta(t)=\theta} \mathcal{D}\theta(t) \exp(-S[\{\theta(t)\}]), \quad (21)$$

where we have introduced the action as

$$S[\{\theta(t)\}] = \int_0^t dt \left[\frac{[(d\theta/dt) - F(\theta)]^2}{4D} + \frac{F'(\theta)}{2} \right]. \quad (22)$$

We may now invoke the Feynman-Kac formalism to identify the path integral on the right hand side of Eq. (21) with the propagator of a quantum mechanical evolution in (negative) imaginary time due to a quantum Hamiltonian H_q . We then have

$$P(\theta, t|\theta_0, 0) = \exp\left(\frac{1}{2D} \int_{\theta_0}^{\theta} F(\theta) d\theta\right) G_q(\theta, -it|\theta_0, 0) = \mathcal{F}(\theta, \theta_0) G_q(\theta, -it|\theta_0, 0), \quad (23)$$

with

$$\mathcal{F}(\theta, \theta_0) \equiv \exp\left(\frac{1}{2D} \left[a(\cos \theta_0 - \cos \theta) + \frac{\cos 2\theta - \cos 2\theta_0}{2} \right]\right), \quad (24)$$

$$G_q(\theta, -it|\theta_0, 0) \equiv \langle \theta | \exp(-H_q t) | \theta_0 \rangle,$$

where the quantum Hamiltonian is

$$H_q(\theta) \equiv -\frac{1}{2m_q} \frac{\partial^2}{\partial \theta^2} + V_q(\theta), \quad (25)$$

the mass in the equivalent quantum problem is

$$m_q \equiv \frac{1}{2D}, \quad (26)$$

and the quantum potential is given by

$$V_q(\theta) \equiv \frac{(F(\theta))^2}{4D} + \frac{F'(\theta)}{2} = \frac{(a \sin \theta - \sin 2\theta)^2}{4D} + \frac{a \cos \theta - 2 \cos 2\theta}{2}. \quad (27)$$

Note that in the quantum propagator in Eq. (24), the Planck's constant has been set to unity.

In terms of the eigenvalues E_n and the eigenfunctions $\Phi_n(\theta)$ of the Hamiltonian $H_q(\theta)$, we have

$$G_q(\theta, -it|\theta_0, 0) = \sum_n \Phi_n(\theta) \Phi_n^*(\theta_0) e^{-E_n t}. \quad (28)$$

Hence, we have

$$P(\theta, t|\theta_0, 0) = \mathcal{F}(\theta, \theta_0) \sum_n \Phi_n(\theta) \Phi_n^*(\theta_0) e^{-E_n t}. \quad (29)$$

In the limit $t \rightarrow \infty$, we may expect that only the eigenvalue equal to zero (provided it exists) will matter, so that we have

$$P(\theta, t \rightarrow \infty|\theta_0, 0) = \mathcal{F}(\theta, \theta_0) \Phi_0(\theta) \Phi_0^*(\theta_0). \quad (30)$$

Equations (29) and (30) constitute our exact expressions for the conditional probability. Obviously, the form of the eigenvalues E_n and eigenfunctions Φ_n depend on the form of the potential $V(\theta)$.

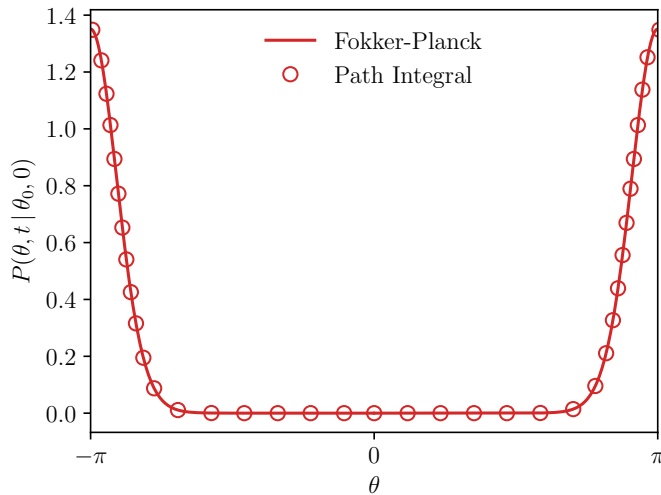


Fig. 5 (Color online) Comparison of the conditional probability $P(\theta, t|\theta_0, 0)$ obtained from the Fokker-Planck and the path integral approach. Here, we have chosen $a = 4$, $D = 0.5$, $t = 5$, $\theta_0 = 0.75\pi$. Note that the probability is peaked at $\theta = \pm\pi$, the stable fixed point at this value of a , see Fig. 2.

In Fig. 5, we show a comparison of the conditional probability $P(\theta, t|\theta_0, 0)$ obtained from the Fokker-Planck and the path-integral approach, for representative values of a, D, t and θ_0 . In the Fokker-Planck approach, we have taken the

truncation parameter to be $n_{\max} = 60$, making sure that higher values do not affect our results appreciably. In the path-integral approach, we obtain the eigenvalues E_n and the eigenfunctions Φ_n of the Hamiltonian (25) by discretizing θ over $[-\pi, \pi]$, expressing the Hamiltonian as a matrix and then solving numerically the corresponding eigenvalue equation. Figure 5 demonstrates an excellent agreement between the results obtained in the two approaches. From the figure, it is evident that the probability is peaked at $\theta = \pm\pi$, the stable fixed point at the considered value of a ; our expectation is that the density $P(\theta, t|\theta_0, 0)$ gets more sharply peaked as $D \rightarrow 0$, thus allowing to recover the stable fixed points of the noiseless dynamics from the noisy one.

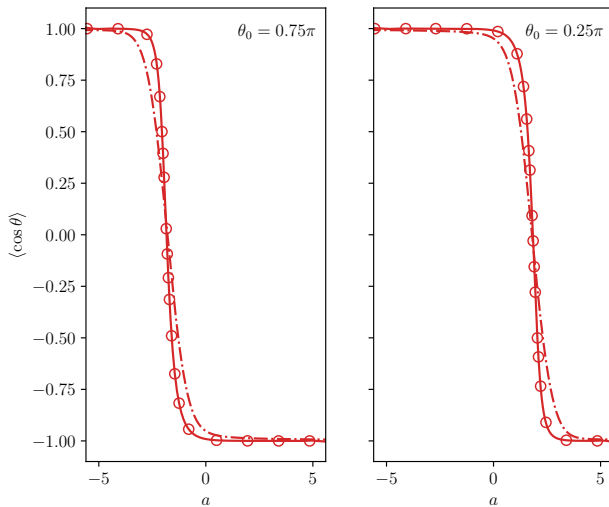


Fig. 6 (Color online) $\langle \cos \theta \rangle$ vs. a at time $t = 1$, and for $\theta_0 = 0.75\pi$ (left panel) and $\theta_0 = 0.25\pi$ (right panel). The lines are obtained by using Eq. (31): The continuous lines are for $D = 10^{-5}$, while the dash-dotted lines are for $D = 10^{-1}$. On the other hand, the circles are obtained by numerically integrating the noiseless dynamics (2) with integration time step $dt = 10^{-3}$. The plots show that the curves corresponding to the noiseless dynamics coincide with the noisy ones in the limit $D \rightarrow 0$.

5 Results and discussions

We now discuss the results obtained from the analysis of the noisy dynamics (3) discussed in the preceding section. For a given initial value θ_0 and a given noise strength D , we may calculate the average of $\cos \theta$ at a given time t and for different values of a by using either the Fokker-Planck or the path-integral result for the conditional probability density $P(\theta, t|\theta_0, 0)$, as

$$\langle \cos \theta \rangle \equiv \langle \cos \theta \rangle(a, D, \theta_0, t) = \int_{-\pi}^{\pi} d\theta \cos \theta P(\theta, t|\theta_0, 0). \quad (31)$$

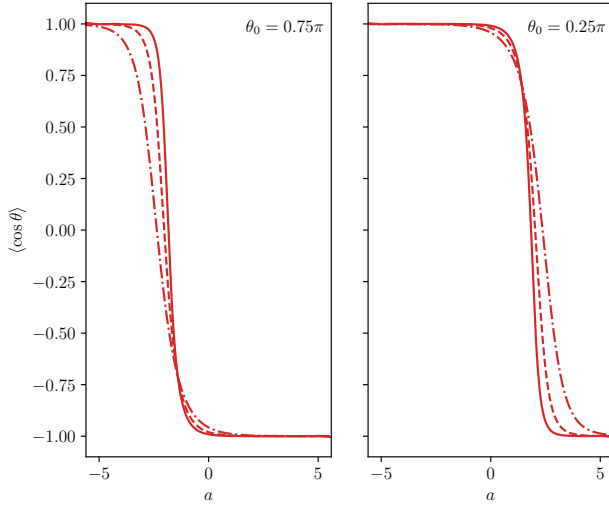


Fig. 7 (Color online) $\langle \cos \theta \rangle$ vs. a for $\theta_0 = 0.75\pi$ (left panel) and $\theta_0 = 0.25\pi$ (right panel). The lines are obtained by using Eq. (31). Here, we have chosen $D = 10^{-5}$. The dash-dotted, the dashed and the continuous line correspond respectively to times $t = 0.6, 0.8, 1.0$. The plots show that the crossover between values $\langle \cos \theta \rangle = +1$ and $\langle \cos \theta \rangle = -1$ with change of a becomes steeper with the increase of t .

Figure 6 shows that the results obtained in the limit $D \rightarrow 0$ (specifically, for $D = 10^{-5}$) are in excellent agreement with the values of $\cos \theta$ estimated from numerical integration of the noiseless dynamics (2). This is consistent with Fig. 4 showing that the noisy trajectories in the limit $D \rightarrow 0$ represent small fluctuations about the trajectories obtained in the noiseless dynamics.

In the next step towards obtaining the bifurcation behavior of the noiseless dynamics from the noisy one, we take $D = 10^{-5}$, and obtain for a given θ_0 and a given time t the behavior of $\langle \cos \theta \rangle$ versus a by using Eq. (31). It is evident from the results shown in Fig. 7 that the cross-over between the two limiting values of $\langle \cos \theta \rangle$, namely, $\langle \cos \theta \rangle = +1$ and $\langle \cos \theta \rangle = -1$, becomes steeper with the increase of t . Indeed, for larger t , one has a sharp jump, as shown in Fig. 8. The same results are obtained as t is increased further, so Fig. 8 characterizes stationary behavior. In this case, we further show that the long-time values of $\cos \theta$ obtained in the noiseless dynamics lie on the curve for the noisy dynamics.

Referring to Fig. 2, for a given θ_0 , consider increasing a from low to high values, that is, moving along a straight line parallel to the x -axis and at a distance θ_0 from it. Then, with change of a , the long-time value of $\cos \theta$ in the noiseless dynamics will be $+1$ so long as the straight line does not intersect the dashed curve in red lying in the region $-2 < a < 2$. Beyond the point of intersection, the long-time value of $\cos \theta$ will be -1 . The point of intersection, obtained by solving $\cos \theta_0 = a/2$, will thus be a crossover point such that for smaller (respectively, larger) a , the stable value of $\cos \theta$ will be $+1$ (respectively, -1). In view of Fig. 6 showing match between the noiseless and the noisy dynamics in the limit of weak noise, such a

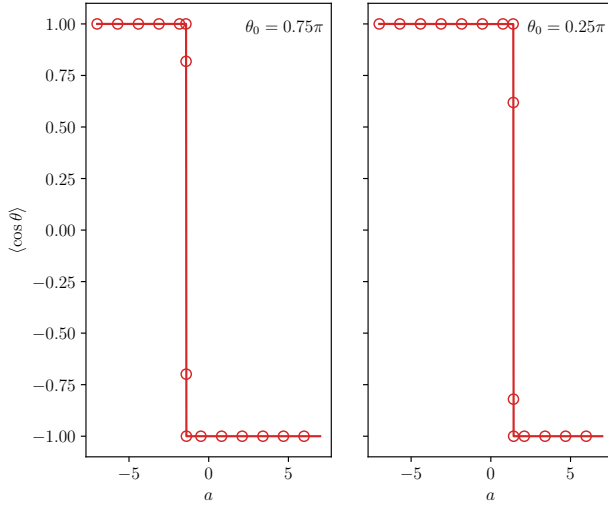


Fig. 8 (Color online) $\langle \cos \theta \rangle$ vs. a obtained in the stationary state (time $t = 10$). The left panel (respectively, the right panel) corresponds to the initial condition $\theta_0 = 0.75\pi$ (respectively, $\theta_0 = 0.25\pi$). Here, we have $D = 10^{-5}$. While the red circles involve using Eq. (31), the lines are obtained from numerical integration of the noiseless dynamics (2) using integration time step $dt = 10^{-3}$.

behavior would be expected of $\langle \cos \theta \rangle$ versus a at long times and is indeed borne out by our exact results shown in Fig. 8. It may be checked from the figure that the crossover point is obtained at the value of a given by $a = 2 \cos \theta_0 = \pm\sqrt{2}$ for the left and the right panel, respectively. Obtaining the crossover point by repeating plots as in Fig. 8 for different values of θ_0 allows to obtain the line of unstable fixed points in the range $-2 < a < 2$. In Fig. 2, we show that as expected, the crossover points so obtained lie exactly on the unstable branch in the range $-2 < a < 2$. Repeating plots as in Fig. 8 for $\theta_0 = 0$ and $\theta_0 = \pi$ allows to obtain the crossover points $a = 2$ and $a = -2$, respectively. These points coincide with the bifurcation points in Fig. 2, thereby explaining the associated stability.

The unstable fixed points of the noiseless dynamics may also be obtained from the noisy dynamics. For example, in order to arrive at the fact that $\theta = 0$ is unstable at $a = 2.5$ (see Fig. 2), one may plot $\langle \cos \theta \rangle$, obtained using Eq. (31), as a function of θ_0 and for different times. From Fig. 9, one may observe that as time increases, $\langle \cos \theta \rangle$ for increasing number of values of θ_0 different from the specific value $\theta_0 = 0$ attains the value of -1 . From the curves for different times, it is evident that in the limit of long times, only when $\theta_0 = 0$ does $\langle \cos \theta \rangle$ have the value of unity, which attains for all other values of θ_0 the value of -1 . This is fully consistent with the bifurcation diagram 2, and has been indicated in the figure by the red circle at $\theta = 0, a = 2.5$.

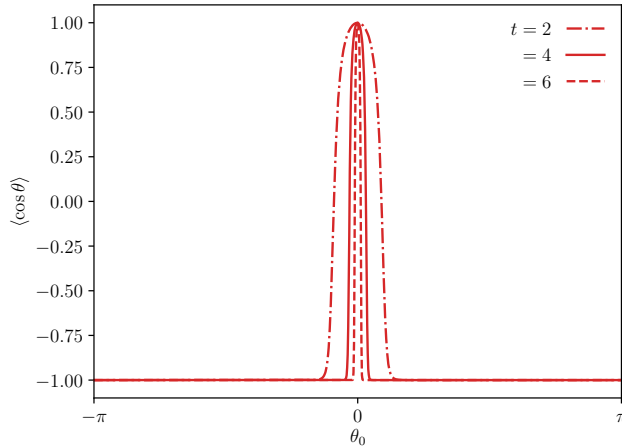


Fig. 9 (Color online) $\langle \cos \theta \rangle$ vs. θ_0 obtained using Eq. (31) and for $a = 2.5$. Here, we have $D = 10^{-5}$, and the different curves correspond to different times t .

6 Conclusions

In this work, we addressed the issue of how one may obtain the bifurcation behavior of a non-linear dynamical system by introducing noise into the dynamics and then studying the resulting Langevin dynamics in the weak-noise limit. Within the ambit of a model system, we showed that a suitable quantity to capture the bifurcation behavior in the noisy dynamics is to define a conditional probability to observe microscopic configurations at a given time while conditioned on observation of a given configuration at an earlier time. The time evolution of the conditional probability may be studied by using two complementary approaches, namely, the Fokker-Planck and the path-integral approach, with the latter yielding exact closed-form expressions for the conditional probability.

The analysis presented in Section 4 applies to any potential $V(\theta)$, and therefore, the whole program of obtaining the bifurcation diagram of a given noiseless dynamics corresponding to a given form of $V(\theta)$ by addition of Gaussian, white noise to the dynamics can be rather straightforwardly carried through. A remarkable feature of the latter approach is that the probability distribution $P(\theta, t|\theta_0, 0)$ obtained from either the Fokker-Planck or the path-integral approach is for weak-enough noise and at long times naturally peaked around the stable fixed points of the noiseless dynamics. In this way, once for a given noiseless dynamics one obtains its fixed points, one may bypass the need to perform a stability analysis of the fixed points in order to locate the stable ones, by studying the corresponding noisy dynamics in the limit of weak noise.

A reason why we could recover the bifurcation behavior in the noisy dynamics is the choice of Gaussian noise for Langevin evolution, which ensures that typical trajectories for the noisy dynamics represent fluctuations of a given size (set by the variance D of the Gaussian distribution for the noise) around the noiseless ones, and hence coincide with the latter in the limit $D \rightarrow 0$. A question that

naturally arises in this regard is: numerically how small should D be? The answer depends on whether one is studying the dynamics around a stable or an unstable fixed point. (a) For a stable fixed point, which corresponds to a local minimum of the potential $V(\theta)$, any reasonably small value of D (smaller than a critical value $D = D_c^{(s)}$) would ensure that almost all trajectories of the noisy dynamics are pushed towards the fixed point by virtue of the potential having a minimum at the stable point, thereby settling into the fixed point at long times. (b) For an unstable fixed point, the issue is a bit tricky. Since such a fixed point corresponds to a local maximum of $V(\theta)$, values of D smaller than $D_c^{(s)}$ that ensured convergence of the noisy to the noiseless dynamics in (a) may prove to be “strong” enough that trajectories starting at the unstable fixed point are pushed away from it to settle into stable fixed points at long times. This would at once invalidate our procedure of obtaining the unstable fixed points of the noiseless dynamics from an analysis of the noisy one. In order that the program is successful, one would be required to reduce further the noise strength, i.e., having a critical value $D_c^{(u)} < D_c^{(s)}$, and considering for convergence values of $D < D_c^{(u)}$.

To illustrate that the aforementioned conclusion is indeed borne out by our results, we show in Fig. 10 the outcome of the following numerical experiment. Referring to Fig. 2, we choose a value of a at which one has a stable fixed point θ^* , and another at which one has an unstable fixed point θ^* , and study the noisy dynamics at these values of a and with the initial value $\theta_0 = \theta^*$. For both, we expect that for D small enough (i.e., for $D < D_c^{(s)}$ (respectively, $D < D_c^{(u)}$) for the stable (respectively, the unstable) fixed point), the long-time value of $\langle \cos \theta \rangle$ should coincide with the value of $\cos \theta^*$. From the figure, we see that indeed we have $D_c^{(u)} < D_c^{(s)}$. Of course, the precision of match between the values of $\langle \cos \theta \rangle$ and $\cos \theta^*$ depends on the precision employed in numerical evaluation of the quantities involved, and higher precision implies lower values of $D_c^{(s)}$ and $D_c^{(u)}$, a fact we have checked in our numerics.

We wrap off by mentioning an utility of studying the noisy dynamics. Any modeling of experimental data on the behavior of a real system by a dynamics should include effects of noise to account for measurement errors. The actual underlying dynamics of course does not have this source of noise, and one is typically interested in inferring how qualitatively different behavior observed in the data obtained with varying experimental parameters emerges from a bifurcation in the actual dynamics. A long-time analysis of the noisy dynamics automatically picks up the stable points of the actual dynamics (experimental data typically contain signatures of only stable points, with unstable points contributing mainly to short-time transients), thus allowing to infer directly the bifurcation behavior of the actual noiseless system from a study of the noisy dynamics.

As a concrete application of our method, we may mention the following scenario: Systems of neurons exhibit diverse dynamical behaviors depending on values of biophysical parameters, such as quiescence, spiking, bursting, and many others. A phenomenological neuron model proposed by Hindmarsh and Rose (the HR model [13]) is known to numerically exhibit all of the above behaviors. Bifurcations in the model as one tunes the various dynamical parameters have been studied mostly numerically or under suitable approximations in specific parameter regimes, owing to challenges involved in pursuing a complete analytical study of the model, see Ref. [14] for a recent study. It will be interesting to see whether adding

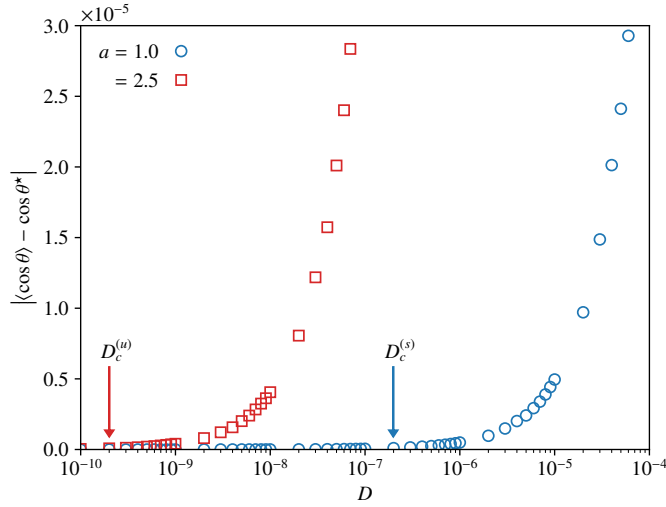


Fig. 10 (Color online) $|\langle \cos \theta \rangle - \cos \theta^*|$ vs. D for values of a at which one has a fixed point at $\theta = \theta^*$. For $a = 1.0$ (respectively, $a = 2.5$), one has a stable (respectively, unstable) fixed point, with $\theta^* = 0$ for both. Here, one obtains $\langle \cos \theta \rangle$ by using Eq. (31) and by choosing $\theta_0 = \theta^*$ and $t = 6$. In the figure, we have indicated the approximate $D_c^{(s)}$ and $D_c^{(u)}$.

noise to the model and studying the resulting noisy dynamics in the weak-noise limit allows to obtain the complete bifurcation diagram of the HR model. It is also left for future work as to how one may extract other features of dynamical systems by studying the corresponding noisy dynamics that allows to use standard tools of statistical physics, e.g., the Fokker-Planck and the path-integral approach.

7 Acknowledgements

The work of Debraj Das is supported by UGC-NET Research Fellowship Sr. No. 2121450744, dated 29-05-2015, Ref. No. 21/12/2014(ii) EU-V. Sayan Roy acknowledges DST-INSPIRE, Government of India for providing him with a scholarship to do a summer project at the Ramakrishna Mission Vivekananda University during May – July, 2018.

References

1. S. H. Strogatz, *Nonlinear Dynamics And Chaos: With Applications To Physics, Biology, Chemistry, And Engineering* (Westview Press, Boulder, 2014).
2. M. Lakshmanan and S. Rajasekar, *Nonlinear Dynamics* (Springer-Verlag, Berlin, 2003).
3. E. Ott, *Chaos in Dynamical Systems* (Cambridge University Press, UK, 2002).
4. M. Cross and H. Greenside, *Pattern Formation and Dynamics in Nonequilibrium Systems* (Cambridge University Press, UK, 2009).
5. T. Dauxois and M. Peyrard, *Physics of Solitons* (Cambridge University Press, UK, 2010).
6. Unless stated otherwise, in this work we use the Euler scheme to perform numerical integration of equations of motion.
7. R. P. Feynman and A. R. Hibbs, *Quantum Mechanics and Path Integrals* (McGrawHill, New York, 2010).

8. L. S. Schulman, *Techniques and Applications of Path Integration* (John Wiley and Sons, Chichester, UK, 1981).
9. M. Kac, *On distribution of certain Wiener functionals*, Trans. Am. Math. Soc. **65**, 1 (1949).
10. M. Kac, *On some connections between probability theory and differential and integral equations*, in *Proc. Second Berkeley Symp. Math. Stat. Prob.* (University of California Press, Berkeley, 1951).
11. C. Gardiner, *Stochastic Methods* (Springer-Verlag, Berlin, 2009).
12. É. Roldán and S. Gupta, *Path-integral formalism for stochastic resetting: Exactly solved examples and shortcuts to confinement*, Phys. Rev. E **96**, 022130 (2017).
13. J. L. Hindmarsh and R. M. Rose, Proc. R. Soc. London, Ser. B **221**, 87 (1984).
14. M. Storaçe, D. Linaro and E. de Lange, Chaos **18**, 033128 (2008).